Accepted Manuscript

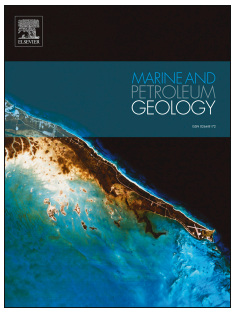

Potential impacts of gas hydrate exploitation on slope stability in the Danube deep-sea fan, Black Sea

Timo Zander, Jung Chan Choi, Maarten Vanneste, Christian Berndt, Anke Dannowski, Brian Carlton, Joerg Bialas

PII: S0264-8172(17)30307-0

DOI: 10.1016/j.marpetgeo.2017.08.010

Reference: JMPG 3027

To appear in: *Marine and Petroleum Geology*

Received Date: 12 May 2017

Revised Date: 4 August 2017

Accepted Date: 9 August 2017

Please cite this article as: Zander, T., Choi, J.C., Vanneste, M., Berndt, C., Dannowski, A., Carlton, B., Bialas, J., Potential impacts of gas hydrate exploitation on slope stability in the Danube deep-sea fan, Black Sea, *Marine and Petroleum Geology* (2017), doi: 10.1016/j.marpetgeo.2017.08.010.

Potential impacts of gas hydrate exploitation on slope stability in the Danube deep-sea fan, Black Sea

Timo Zander[1], Jung Chan Choi[2], Maarten Vanneste[2], Christian Berndt[1], Anke Dannowski[1], Brian Carlton[2], Joerg Bialas[1]

[1]Geomar Helmholtz Centre for Ocean Research Kiel, Wischhofstraße 1-3, 24148 Kiel, Germany

[2]Norwegian Geotechnical Institute (NGI), Oslo, Norway

Corresponding Author: Timo Zander, tzander@geomar.de

Keywords: Black Sea, slope stability, gas hydrates, gas hydrate production, geohazard assessment

Abstract

Methane production from gas hydrate reservoirs is only economically viable for hydrate reservoirs in permeable sediments. The most suitable known prospect in European waters is the paleo Danube deep-sea fan in the Bulgarian exclusive economic zone in the Black Sea where a gas hydrate reservoir is found 60 m below the seafloor in water depths of about 1500 m. To investigate the hazards associated with gas production-induced slope failures we carried out a slope stability analysis for this area. Screening of the area based on multibeam bathymetry data shows that the area is overall stable with some critical slopes at the inner levees of the paleo channels. Hydrate production using the depressurization method will increase the effective stresses in the reservoir beyond pre-consolidation stress, which results in sediment compaction and seafloor subsidence. The modeling results show that subsidence would locally be in the order of up to 0.4 m, but it remains confined to the immediate vicinity above the production site. Our simulations show that the Factor of Safety against slope failure (1.27) is not affected by the production process, and it is more likely that a landslide is triggered by an earthquake than by production itself. If a landslide were to happen, the mobilized sediments on the most likely failure plane could generate a landslide that would hit the production site with velocities of up to 10 m s^{-1}. This case study shows that even in the case of production from very shallow gas hydrate reservoirs the threat of naturally occurring slope failures may be greater than that of hydrate production itself and has to be considered carefully in hazard assessments.

1. Introduction

Gas hydrates are ice-like crystals that occur in large quantities along continental margins and permafrost regions. Their stability depends on high pressure and low temperature as well as on salinity and gas composition (Shipley et al., 1979). In the marine environment, gas hydrates primarily consist of methane and dominantly form in crystallographic structure I (e.g. Sloan, 1998).

Gas hydrates are considered a potential energy resource and research programs in several countries including Japan, Korea, and India are dedicated to the exploration and ultimately the exploitation of offshore gas hydrate reservoirs. The German SUGAR project aims at developing technologies for the exploration and exploitation of methane hydrates within European waters. Economically viable hydrate reservoirs occur in sands and coarse silts with permeability that is high enough to sustain gas flow towards the well during production. The paleo Danube deep-sea fan in the Black Sea offers the best conditions for hydrate production in Europe because it contains sandy sediments and a widespread bottom simulating reflector (BSR) in seismic data that indicates the presence of gas hydrates (Popescu et al., 2006, Zander et al., 2017).

Several production technologies have been considered to produce methane from gas hydrates. All are based on the dissociation of hydrates following a gas flow towards a production well. Applicable methods include warming of hydrated sediments by injection of warm water and chemical stimulation of methane hydrate with an agent such as nitrogen, methylene or carbon dioxide. However, the economically most favorable production method is depressurization (Fig. 1). The concept of depressurization was applied and validated in a production test in the Nankai Trough offshore Japan in 2013 (Yamamoto et al., 2014). Studies showed that the high bottom water temperature of around 9 °C in the Black Sea is not conducive to hydrate dissociation by CO_2 or N_2 injection, while such high temperatures increase the efficiency of the depressurization method (Merey and Sinayuk, 2016a).

The basic concept of the depressurization method involves a borehole which is drilled vertically into the gas hydrate reservoir, and pressure reduction by pumping along the entire reservoir interval. Pressure reduction forces hydrate dissociation, which gradually spreads out from the well into the surrounding hydrate reservoir. Typically, the pore pressure around the well is reduced to a specific target (e.g. 2.7 MPa at Walker Ridge (Myshakin et al., 2012) and 3 MPa at Nankai (Yamamoto et al., 2014)). Models showed that a pressure target of 3 MPa

yields the highest gas production in Black Sea sediments (Merey and Sinayuc, 2016b). In 1500 m water depth, this pressure reduction is comparable to a sea level fall of 1200 m. The area affected by pressure reduction is expected to remain relatively limited to the vicinity of the well location, i.e., 100 m around the well (Kvalstad et al., 2011).

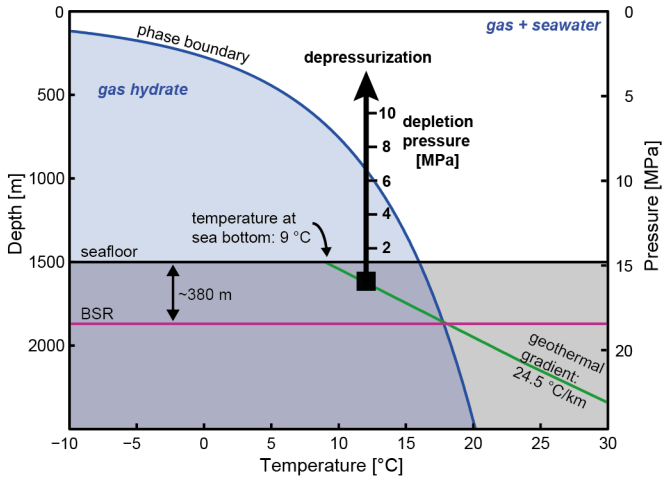

Fig. 1: Gas hydrate phase diagram showing the gas hydrate stability zone in the upper ~380 m below the seafloor and the pressure path during gas hydrate dissociation under pressure reduction (black arrow).

Following depressurization, hydrate dissociation in the sandy sediments will cause an increase in permeability. Hydrates typically are load-bearing and grain-supporting when their saturation exceeds 25 – 40 % (Waite et al., 2009). Thus, the disappearance of the cementing hydrates will typically lead to a softening of the sediments. Consequently, the effective stress in the reservoir will increase, which leads to sediment compaction towards the dissociation area in all directions (Zhou et al., 2014). Simulations showed that the radial displacements are smaller than the vertical displacements, with the latter being largest directly above the production zone and close to zero underneath the production zone (Zhou et al., 2014). As a result, gas production from a shallow compacting reservoir may cause subsidence at the seafloor (Fjaer et al., 2008, Kim et al., 2014).

One of the most important offshore geohazards is submarine slope failure (Vanneste et al., 2014). Areas with steep slopes, caused, e.g. by submarine channels such as those encountered in the Danube deep-sea fan, are more susceptible to slope failure than the

surrounding areas (Kvalstad, 2007). Instable slopes may cause sliding or slumping of the seafloor sediments, and even on gently dipping slopes mobilized mass can travel over large distances during a landslide. Sediment failure occurs when the shear stress (e.g. the gravitational downslope force) exceeds the shear strength (resisting forces). The initiation of seabed failures can be triggered by both natural causes and human interference such as over-steepening of the slope, uneven deposition or erosion, increase of shear stress (loading, lateral pressure), reduction of shear strength, and seismic events (lateral and vertical ground shaking due to earthquakes). So far it remains unclear whether natural gas hydrate dynamics have triggered slope failures. A review of landslide inventories carried out by Urlaub et al. (2013) did not find evidence for a large-scale triggering of landslides due to gas hydrate dissociation caused by the glacial-interglacial pressure and temperature changes. Nevertheless, gas hydrate dissociation may be considered as a preconditioning mechanism instead of an actual trigger for certain submarine landslides (Kwon and Cho, 2012; Crutchley et al., 2016) and there is evidence that some submarine landslides have developed differently in areas with hydrate than in those without (Micallef et al., 2009). The transported mass of a submarine landslide can affect installations in various forms such as loss of foundation area, debris impact causing destruction of facilities, or even partial or total burial of seabed facilities, and generation of tsunamis affecting coastal communities over potentially large areas (Kvalstad, 2007).

In this study, we focus on a part of the paleo Danube deep-sea fan which has been investigated with various geophysical tools in the German SUGAR project to investigate its suitability as a gas hydrate production test site. Our aim is to find out if production of gas from a shallow hydrate reservoir can be performed safely at this location, particularly with respect to slope stability. The objectives are (i) to identify slopes with the lowest Factor of Safety (FoS) near the target area and to assess whether the slope in this area can be considered stable; (ii) to simulate hydrate production in a 2D slope stability model to constrain the amount and timing of expected slope deformation; and (iii) to determine the run-out distance

and potential implications for infrastructure and installations at the production site through simulation of a landslide along the most critical segment of the slope as modeled in the previous step.

2. Geological Setting

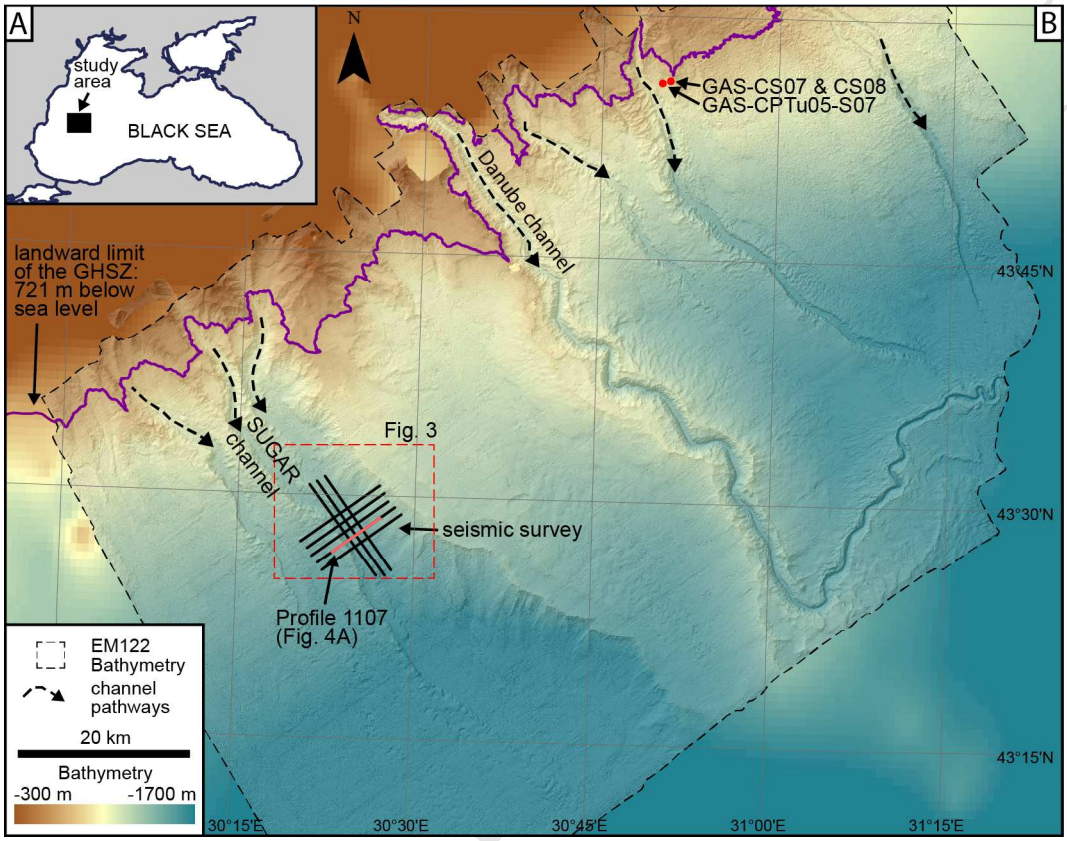

Fig. 2: Bathymetric map (25 m x 25 m resolution) of the Danube deep-sea fan in the Black Sea. Note the prominent channel-levee systems, which transport sand into the study area. This sand provides the host rock for the gas hydrate accumulations.

The continental shelf of the northwestern Black Sea basin is up to 120 km wide. During the last glaciation, the rivers Danube, Dniepr, Dniestr and Bug discharged large amounts of sediments off the shelf break at about 100 m water depth down to the abyssal plain at 2200 m water depth (Wong et al., 1997). The depositional areas, which constitute the paleo Danube and Dniepr deep-sea fans, are characterized by numerous canyons and channels (Fig. 2), which formed by erosion on the upper slope and by deposition on the middle and lower slope (Popescu et al., 2001). These canyons and channels formed additional slopes along their courses. The highest slope angles typically occur along the inner levee walls of

channel-levee systems (Hansen et al., 2015). As observed in other river fans of the northern hemisphere, the right-hand (western) levees are more pronounced than the left-hand (eastern) levees because of the Coriolis force (Popescu et al., 2001). Several older channels can be identified from the bathymetry, such as a channel westwards of the Danube channel which was named SUGAR channel (Fig. 2; Zander et al., 2017).

For the observed bottom water temperature of 9 °C (Degens and Ross, 1974) and a salinity of 22.3 (Özsoy and Ünlüata, 1997) the upper limit of the gas hydrate stability zone is located at a water depth of 721 m. The pore water salinity decreases rapidly in shallow depth below the seafloor to a level of 3-5 (Soulet et al., 2010), which shifts the phase boundary for methane hydrates upwards. Indirect indicators for gas hydrates exist in the form of a BSR which is observed in reflection seismic data (Popescu et al., 2006; Zander et al., 2017), and gas hydrate was sampled during a research cruise in 2015 (Ker and Riboulot, 2015). Anomalous multiple BSRs were identified in the levees of a buried channel-levee system underneath the SUGAR channel. These additional BSRs are caused by changes in pressure and temperature conditions during the glacial cycle and indicate that the Danube area is not in a steady state (Zander et al., 2017).

The SUGAR project targets a potential gas hydrate reservoir at the base of the SUGAR channel in about 1500 m water depth. Preliminary results of controlled source electromagnetic (CSEM) data (Schwalenberg et al., 2016) and a shear wave anomaly observed in ocean bottom seismometer (OBS) data (Dannowski et al., 2016) suggest a shallow zone (~60 m depth) of increased gas hydrate saturation with potentially up to 40% hydrate concentration in the pore space.

3. Data and Methods

Slope stability assessments are generally based on a conservative scenario. To get an idea of the stability of a given slope, the slip zone with the least FoS in static models is determined. The FoS is defined as resisting forces against driving forces, and theoretically a

slope with a FoS of less than 1.0 is prone to fail. However, because of uncertainties due to simplified modeling and parameter variations, a FoS of 1.5 is generally used to define a stable slope, but this depends on the infrastructure at risk as well as local standards and guidelines (CEN, 2004). Pseudo-static models are additionally applied to simulate seismic effects. Under pseudo-static condition, a minimum FoS of 1.1 is generally required. Note that typically a full dynamic site response analysis is preferred over pseudo-static models.

The constraints for geomechanical models and slope stability analyses ideally comprise the geometry of the slope, the geology of the subsurface, strength parameters of the soils and the unit weights. However, for this study, not all of these input parameters were available due to a limited number of boreholes and the complexities of measuring the strength of weak soils. Furthermore, the sampling program was not ideal for geotechnical analyses as only academic methods were available. We therefore used simplified scenarios and approximate some of the parameters. On the other hand, our high-resolution 2D seismic data are excellent, with resolution two to three times better than the resolution of common industry-type 3D seismic data, as the survey focused on the upper 500 m of gas hydrate-hosting sediments. Seismic and bathymetry data were collected during cruise MSM34 onboard the German research vessel MARIA S. MERIAN from December 2013 to January 2014 (Bialas et al., 2014).

3.1 Multibeam bathymetry

Multibeam bathymetry data were collected using the ship-mounted EM122 echosounder (Kongsberg). The resulting maps are based on a grid of 25 m x 25 m bin size for the Danube deep-sea fan survey (Fig. 2) and 10 m x 10 m bin size for the study area (Fig. 3).

3.2 2D reflection seismic data

A 2D high-resolution multichannel seismic survey was conducted using a 62.6 m-long streamer with 40 channels and a group distance of 1.56 m. Eight profiles were recorded over an area of two merging channel-levee systems: three profiles along the channel’s direction (14

km length each), and five across the channel (11 km length each) (Fig. 2). A 45/45 in^3 GI gun was used as a source with a shot interval of 5 s. After navigation processing, Omega (WesternGeco) was used for signal processing, stacking, and amplitude-preserving time migration. No gain was applied during processing. Due to the short streamers, velocity data could not be derived and had to be extrapolated from other seismic data discussed in a previous study (Zander et al., 2017). These extrapolated velocities were cross-checked with P-wave velocities derived from OBS stations that were also deployed in the study area (Dannowski et al., 2016). We used these data to convert the seismic data from time to depth domain.

3.3 Soil properties

Only very sparse geotechnical and geomechanical data are available from the Black Sea, and to our knowledge, no such data exist for the target area itself. Our 2D slope stability model is therefore based on two different soil parameter sets: one for the gas hydrate reservoir and one for the surrounding sediments (in the following referred to as the overburden). Due to the rather uniform sedimentation in the top 10 m – 30 m of sediments in the Black Sea (e.g. Ross and Degens, 1974; Soulet et al., 2010; Bialas et al, 2014), we decided to estimate the overburden soil parameters from measurements taken during a cruise onboard the RV Pourquoi Pas? in 2015, which was carried out in the northeastern part of the Danube deep-sea fan in Romanian territory (Ker and Riboulot, 2015, Garziglia, 2016). The reservoir's soil parameters were estimated based on published parameters from the successful hydrate production test site in the Nankai Trough offshore Japan (Santamarina et al., 2015; Yoneda et al., 2015). The hydrate reservoir in the Nankai area is located in the sandy channel bed deposits of a buried channel-levee system about 300 m below the seafloor in a water depth of about 1 km (Saeki et al., 2008).

3.3.1 Overburden

In 2015, piezocone and pore pressure data were collected in the Romanian territory of the Danube deep-Sea fan in a water depth of 729 m, at the top of a bathymetric high running N-S along a distance of 3 km with a maximum height of about 50 m above the surrounding area (Fig. 2) (Ker and Riboulot, 2015). The results obtained from triaxial tests on cores GAS-CS07 and GAS-CS08 were used for correlation with the cone penetration test GAS-CPTu05-S07 (Garziglia, 2016; and pers. communication). The overburden was assumed to behave as undrained since the piezocone data identified the sediment overburden as clay. The mechanical behavior of the overburden was thus modeled using an elasto-perfectly plastic model with undrained shear strength varying with depth. The model considered a depth varying stiffness/compressibility using the rigidity index, which is the ratio of shear modulus to undrained shear strength. The overburden soil properties used in this study are summarized in table 1.

Table 1: Overburden soil parameters (Garziglia, 2016; and pers. communication). γ is the total unit soil weight, G is the shear modulus, s_u is the undrained shear strength, $\sigma'v$ is the effective vertical in-situ stress. The locations of the cores are shown in Fig. 2.

Parameter	Notation	Value	Reference
Total unit soil weight	γ	17.5 kN m^{-3}	
Rigidity index	G/s_u	140	GAS-CS07, GAS-CS08
Poisson's ratio	ν	0.49	
Undrained shear strength ratio	$s_u/\sigma'v$	0.4	GAS-CPTu05-S07

3.3.2 Gas hydrate reservoir

Shear strength and elastic stiffness of sandy hydrate-bearing sediments are sensitive to hydrate saturation and confining pressure (Yoneda et al., 2015). Extensive laboratory test programs were carried out in the Nankai Trough, where gas production from hydrates was tested successfully (Yamamoto et al., 2014). The results show that the shear strength and elastic stiffness tend to increase with the hydrate saturation. Strengthening is most likely caused by the cohesion induced by hydrate bonding (Santamarina et al., 2015, Yoneda et al., 2015). To obtain realistic parameters for the hydrate reservoir in the Black Sea target area, the

material properties of the studied area were thus calibrated as a function of hydrate saturation and the in-situ stress condition (Yoneda et al., 2015). The input properties applied in this study are summarized in Table 2.

Table 2: Parameters for the geotechnical model of the gas hydrate reservoir based on laboratory tests on borehole samples from the Nankai Trough (obtained from Santamarina et al., 2015 and calibrated through relations published in Yoneda et al., 2015). Mbsf = meter below seafloor.

Depth [mbsf]	Confining stress [MPa]	Saturation	E50 [MPa]	Poisson's ratio	Shear modulus [MPa]	Cohesion [MPa]	Friction angle [°]
60	~0.35	Before dissociation					
		0.4	100	0.22	41	1.5	25-30
		After dissociation					
		0	80	0.22	32.8	0 – 0.5	25-30

3.4 Slope stability screening tool

In order to select a potentially unstable area and suitable transects to perform a 2D slope stability analysis, a screening of the area based on bathymetric data and geotechnical soil parameters was performed within the top 30 m of soil. The functionality of the screening tool is described in Carlton et al. (2017). The tool estimates the FoS using the infinite slope method (Morgenstern, 1967) and the probability against failure using the First Order Second Moment (FOSM) method. For our simplified soil model parameters, the FoS decreases with depth below the surface, and is largely controlled by the slope angle. Additionally, seismically induced permanent displacements are calculated in the pseudo-static slope stability analysis.

Table 3: Input parameters for the screening tool. s_u is the undrained shear strength.

Parameter	Notation	Value	Reference
Maximum depth below seafloor of the analysis	Z_{max}	30 m	-
Coefficient of variation of k	COV_k	0.2	-
Momentum magnitude	M_w	7.2	Matova, 2000
Peak ground acceleration	PGA	0.1	GSHAP (Giardini, 1999)
Pseudo-static coefficient	k	0.5 PGA	Hynes-Griffin and Franklin, 1984
Pore pressure ratio	r_u	0	-
Coefficient of variation of s_u	COV_{su}	0.2	-

3.5 2D geomechanical analysis

The numerical 2D static geomechanical analysis provides key information on the static and pseudo-static FoS as well as the deformation of the subsurface during hydrate dissociation. The numerical analysis calculates both the most likely failure plane and the volume of sediment that may fail. The simulation was carried out using the commercial finite element software PLAXIS 2D (Brinkgreve et al, 2007). The overburden was modeled with an elasto-perfectly plastic model and the Mohr-Coulomb model was used for the reservoir to capture mechanical deformation. The FoS was calculated by reducing the shear strength parameters until the soil mass failed, which is known as the 'phi-c reduction method' (Griffiths and Lane, 1999). Variations in terrain and stratigraphy were derived from the interpretation of the 2D seismic profiles, and soil strength parameters were incorporated. The software first calculated the slip zone with the least FoS against sliding. The production of methane out of a methane hydrate reservoir was then simulated by reducing the pressure and changing the reservoir's material properties given in Table 2 within a certain range. The FoS was then calculated again to determine any change of slope stability due to a potential change in topography resulting from seafloor subsidence as well as changes in shear strength in the subsurface. In addition to the simulation under static conditions, a pseudo-static simulation was carried out which included horizontal forces caused by earthquake loading.

3.6 Landslide dynamics simulation

Landslides due to hydrate exploitation were modeled to assess the potential run-out distance and velocities for a downslope travelling landslide from the adjacent steep levee walls. The analysis will help to determine potential mitigation measures (e.g. relocation options, design criteria) that may need to be considered for the production infrastructure at the sea bottom.

For the run-out simulations, we used a propriety NGI code for visco-plastic flows in quasi-2D (i.e. depth-averaged). The code is based on the BING code from St. Anthony Falls

Laboratory (Imran et al., 2001) and the various extensions to this code were described by De Blasio et al. (2004). The BING3 model performs an analysis of the run-out of an arbitrarily shaped slide block along a predefined geometry (extended slip plane). The model is specifically developed for submarine conditions. The code is based on a non-linear Herschel-Bulkley rheology coupled with depth-averaged mass and momentum continuity equations that were solved using a Lagrangian scheme. The model includes hydrodynamic pressure and friction drag during run-out as well as strength degradation, and can also be used for debris flows with embedded rafted blocks (e.g., Vanneste et al., 2011). Further options are hydroplaning and erosion or entrainment of seabed material, but we did not use these options as there was too little information on the boundary conditions.

The results of the 2D slope stability model from PLAXIS (for both static and pseudo-static analysis) were used as input for the landslide dynamics modeling to guarantee consistency of the results. As there is significant uncertainty on the soil properties, we have run several simulations using a range of realistic soil parameters (Table 4). The most critical parameters are:

$\tau_{y,s}$ Initial yield strength of the soil at the time of failure (kPa)

$\tau_{y,r}$ Fully remolded yield strength of the soil (kPa)

R_c Remolding coefficient, with a high value corresponding to rapid remolding during the flow (-)

ν Kinematic viscosity at the flow node ($m^2\ s^{-1}$)

n Herschel-Bulkley exponent (n = 1 implies Bingham fluid)

C_P Pressure drag coefficient, -

C_{FR} Friction drag coefficient, -

In principle, these properties may vary at each node, but we used constant values. We also kept the density of the slurry constant at 1680 kg m^{-3}. We ran the model with a 5 m cell length for the flow, following stability testing. The same properties were used for the static

and pseudo-static cases. The parameter range was constrained from either the limited site-specific data of NGI's soil data base for similar soil types as well as the results from the screening tool and PLAXIS simulations. The parameter range includes relatively weak as well as relatively strong conditions, representing end-members for the simulation.

Results of the run-out simulations are: (1) final deposit (thickness) of the mass along the flow path; (2) toe velocity during the flow; (3) peak height at each point along the flow path and (4) peak velocity at each point along the flow path. Limitations are that lateral spreading cannot be taken into account in this quasi-2D model, as a result, the landslide velocity and peak heights may be overestimating high.

Table 4: Input parameters for the landslide dynamics simulation. $\tau_{y,s}$ = initial yield strength of the soil at the time of failure, $\tau_{y,r}$ = fully remolded yield strength of the soil, R_c = remolding coefficient, with a high value corresponding to rapid remolding during the flow, ν = Kinematic viscosity at the flow node, n = Herschel-Bulkley exponent, C_P = Pressure drag coefficient, C_{FR} = Friction drag coefficient

model	$\tau_{y,s}$	$\tau_{y,r}$	R_c	ν	n	C_P	C_{FR}
	kPa	kPa	-	m2 s^{-1}	-	-	-
1	0.75	0.75	0	0.237	0.25	1	0.001
2	4.50	4.50	0	0.237	0.15	1	0.001
3	3.00	3.00	0	0.237	0.15	1	0.001
4	3.00	3.00	0	0.237	0.35	1	0.001
5	3.00	3.00	0	0.400	0.35	1	0.001
6	4.50	1.50	0.0001	0.237	0.15	1	0.001
7	4.50	0.75	0.001	0.500	0.15	1	0.001
8	4.50	0.75	0.01	0.500	0.15	1	0.001
9	4.50	0.75	0.001	0.500	0.25	1	0.001
10	4.50	0.75	0.001	0.500	0.35	1	0.001
11	3.00	0.75	0.001	0.300	0.15	1	0.001
12	7.50	1.50	0.001	0.300	0.15	1	0.001
13	4.50	1.88	0.001	0.250	0.15	1	0.001
14	4.50	1.88	0.001	0.250	0.15	1	0.001
15	4.50	2.25	0.001	0.250	0.15	1	0.001
16	7.50	2.25	0.0001	0.250	0.15	1	0.001
17	7.50	2.25	0.005	0.250	0.15	1	0.001
18	4.50	0.60	0.001	0.500	0.15	1	0.001
19	11.20	2.80	0.01	2.400	0.15	0.5	0.005
20	11.20	2.80	0.01	0.600	0.15	0.5	0.005
21	11.20	2.80	0.01	0.300	0.15	0.5	0.005
22	11.20	2.80	0.1	2.400	0.15	0.5	0.005

23	11.20	2.80	0.1	0.300	0.15	0.5	0.005
24	11.20	2.52	0.1	0.300	0.15	0.5	0.005
25	11.20	2.10	0.1	0.300	0.15	0.5	0.005
26	11.20	1.40	0.01	2.400	0.15	0.5	0.005
27	11.20	1.40	0.1	2.400	0.15	0.5	0.005

4. Results

4.1 Initial screening

Fig. 3B and Fig. 3C show the slope attribute and the deterministic minimum FoS under static condition, respectively. This is based on the 10 m x 10 m bathymetry dataset (Fig. 3A) and the parameters in Tables 1 and 3. In the study area, any area with slope inclinations exceeding 9° has the potential for slope failure as the associated deterministic FoS falls below 1.5. Most steep natural slopes are located along the paleo-channels at the inner levee walls, especially on the western levees (Fig. 3B). Under static conditions, some segments along the levee flanks appear critical with FoS lower than 1.5 (Fig. 3C). Because of the low FoS in the static case, we ran an additional pseudo-static slope stability analysis in which an inertial horizontal force was added to represent the effect of earthquake shaking. Earthquakes that triggered tsunamis happened in this area, such as the 1901 Black Sea earthquake with estimated magnitude of 7.2 (Matova, 2000). The simulation showed that for the pseudo-static screening, the critical areas around the levee walls are larger compared to the static case (Fig. 3D).

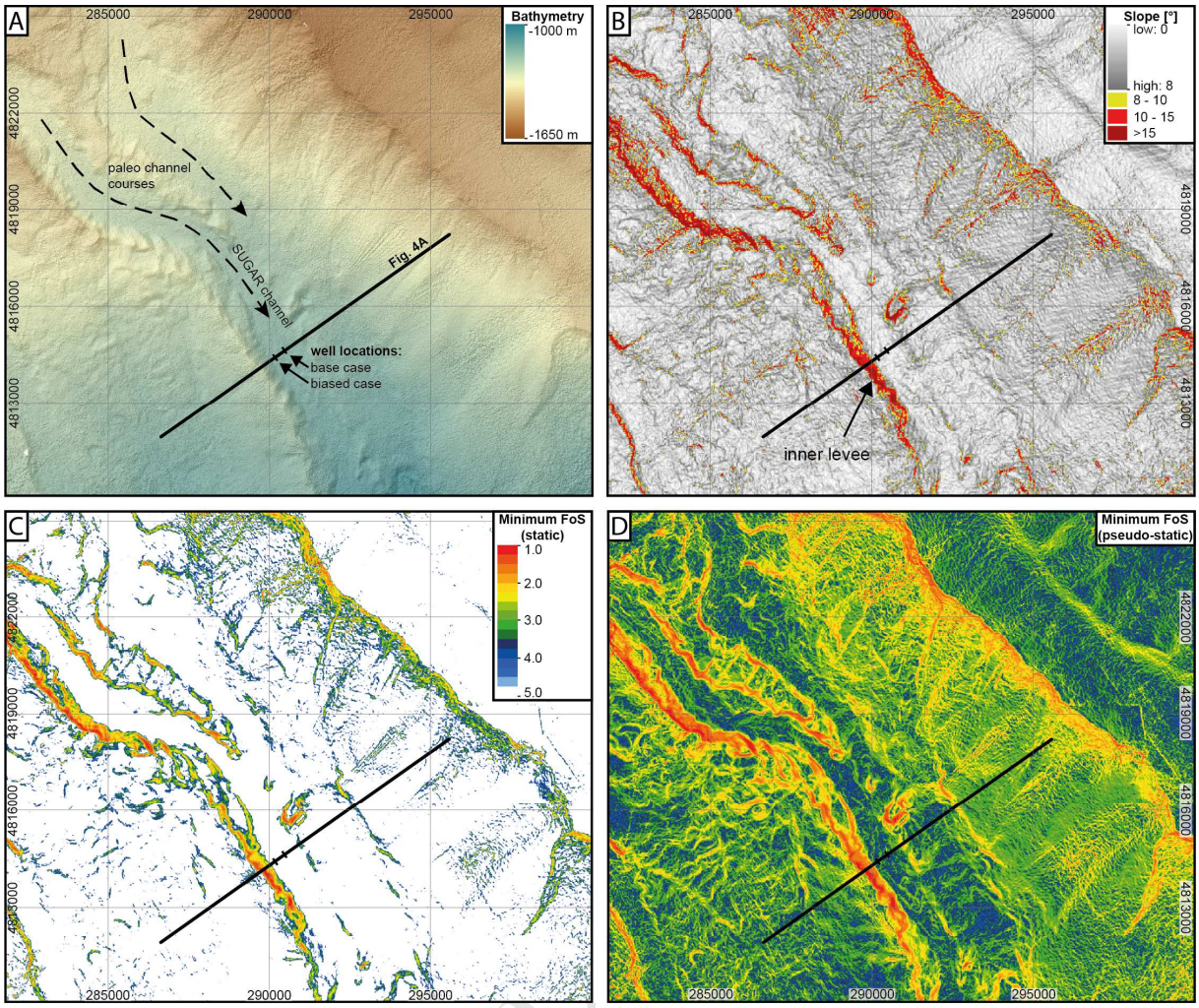

Fig. 3 A: Shaded relief bathymetry data from the study area. B: Slope angle calculated from the bathymetry data. C: Minimum Factor of Safety (FoS) under static conditions in the top 30 m of soil. D: Minimum FoS under pseudo-static conditions in the top 30 m of soil. The color scale is the same as in C. Coordinates are given in UTM zone 36N, the location is shown in Fig. 2.

4.2 2D geomechanical analysis

Based on the screening results, we identified the western levee of the SUGAR channel as the most critical area in terms of slope stability (Fig. 3B). We therefore selected the seismic profile 1107, which crosses perpendicular to the levee slope and coincides with the area where most of the geophysical data were collected (Fig. 3). The geometry for the 2D geomechanical model was constrained from seismic interpretation and picking of prominent seismic horizons. In the seismic data, the channel facies of the most recent active channel system is clearly visible (Fig. 4A). At a depth of about 60 m below the channel seabed, a high amplitude reflection marks the base of the SUGAR channel. The levee at the western channel margin is characterized by well stratified seismic reflections. We interpret this seismic facies

as overbank deposits that typically consist of fine-grained mud, clay and silt (Damuth, 2002). In contrast, the base of a channel-levee system typically consists of coarse-grained sand and gravel (Damuth, 2002), which would provide ideal conditions for the exploitation of gas hydrates out of the pore space by using the depressurization method (e.g. Boswell, 2009).

Gas hydrates cannot be directly identified in reflection seismic data. However, seismic studies (Dannowski et al. 2016) and CSEM studies (Schwalenberg et al. 2016) conducted in the study area found indications for gas hydrates as shallow as 50 m below the seafloor with gas hydrate saturation up to 40 %. The thickness and spatial extent of this potential gas hydrate reservoir is still under debate and will require confirmation through drilling in the future. For this study and based on the observations and results mentioned above, we assumed a thin gas hydrate reservoir along the high-amplitude reflector at the base of the SUGAR channel. This shallow reservoir has an average thickness of about 6 m. In addition, we defined a second hypothetical gas hydrate reservoir following a distinct reflector at a depth of about 140 m below the seafloor and with a thickness of 30 m (Fig. 4a). This second reservoir served to assess the effect of reservoir depth on subsidence due to hydrate production. The base of the hydrate stability zone is about 380 m below the seafloor at this location (Figs. 1 and 4A).

The finite element model built in PLAXIS 2D was composed of 19,352 10-noded triangular elements. To minimize discretization effects and to capture the failure mechanism, the element size was gradually refined close to the reservoir (Fig. 4C). The soil parameters described in section 3.3.1 were applied to the overburden soils. To assess the present-day stability of the area, we initially calculated the slip zone with the least FoS under static conditions. The calculated slip plane is located at the steepest part of the levee, and has a horizontal length of about 120 m and a maximum thickness of 15 m, with a FoS of 1.27 (Fig.4B). In the pseudo-static slope stability analysis, the slip plane is located slightly deeper at about 17 m and has a larger extent of about 140 m. The FoS is lower at about 1.01.

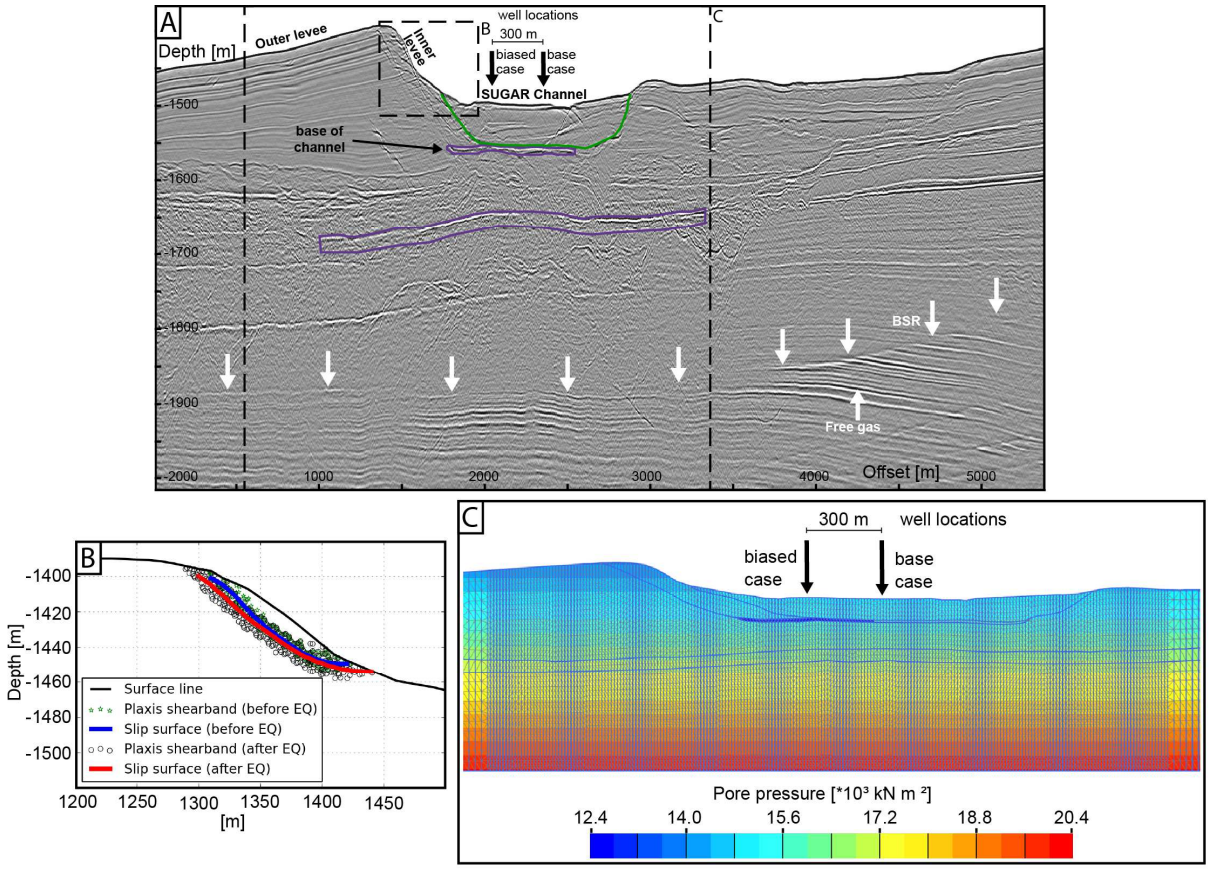

Fig. 4. A: 2D line 1107 across the SUGAR channel-levee system, which is located well above the base of the gas hydrate stability zone indicated by the BSR (white arrows) in about 380 m depth below the seafloor. The two hypothetical gas hydrate reservoirs (purple polygon) are located in about 60 m depth at the base of the most recent active channel (shallow reservoir), and in a depth of about 140 m (deeper reservoir). Green = outline of the SUGAR channel. The location of the profile is shown in Fig. 3. B: Comparison of the best-fit slip planes obtained from the shear bands under static and pseudo-static conditions. C: Total pore pressure distribution in the finite-element model based on the profile in A, with potential positions of the wells considered in this study.

4.3 Effect of hydrate production on slope stability

In order to simulate gas production out of the hypothetical reservoirs, we investigate various production scenarios as a parametric study. This study focuses on the shallow hydrate reservoir, as there is more evidence for the presence of hydrate in this reservoir compared to the deeper target and because any effects on seafloor stability are expected to be stronger for the shallower reservoir. First, a well location was defined. The pore pressure at the well was then depleted along the entire vertical thickness of the reservoir. Within the depleted zone, the pressure was kept constantly low and the dissociation front spread out gradually into the reservoir over time. The pressure reduction was considered as 8 to 10 MPa based on the field

scale production test in the Nankai Trough (Konno et al., 2017), which is sufficiently high for hydrates to dissociate under the pressure and temperature conditions in the study area (Fig. 1).

We tested the following scenarios:

- Depletion pressures of 8 MPa and 10 MPa
- 10 m to 150 m radius around the borehole for the area affected by hydrate dissociation indicative for the production time
- Well location at the center of the SUGAR channel (base case) and closer to the levee (biased case)
- production out of the shallow reservoir and production from the deeper reservoir.

4.3.1 Depletion pressure increase

Fig. 5 shows the effect of different depletion pressures on reservoir compaction and subsidence. For this parameter test, we assumed that constant pore pressure reduction affects the reservoir within 150 m around the well. The maximum depletion pressure (10 MPa in the entire dissociation zone) is representative for a target of 12 MPa depletion at the well. A simulation carried out in the Ulleung Basin of the Korean East Sea showed that the pressure target will only be achieved in a very narrow zone close to the well and decreases rapidly towards the margin of the reservoir (Kim et al., 2014), and similar results were shown for the production site in the Nankai Trough (Konno et al., 2017). The geomechanical simulation showed that higher depletion pressure increases the mean compaction rate of the reservoir, with a maximum compaction of 0.69 m for a 10 MPa depletion.

The subsidence at the seafloor is about 30 % smaller compared to the reservoir compaction, with a maximum subsidence of 0.41 m for the 10 MPa depletion case. The lateral extent of the deformation at the seabed is limited to the vicinity of the compacted reservoir and does not spread out to the failure surface at the levee margin. The FoS of the slip surface remains unaffected.

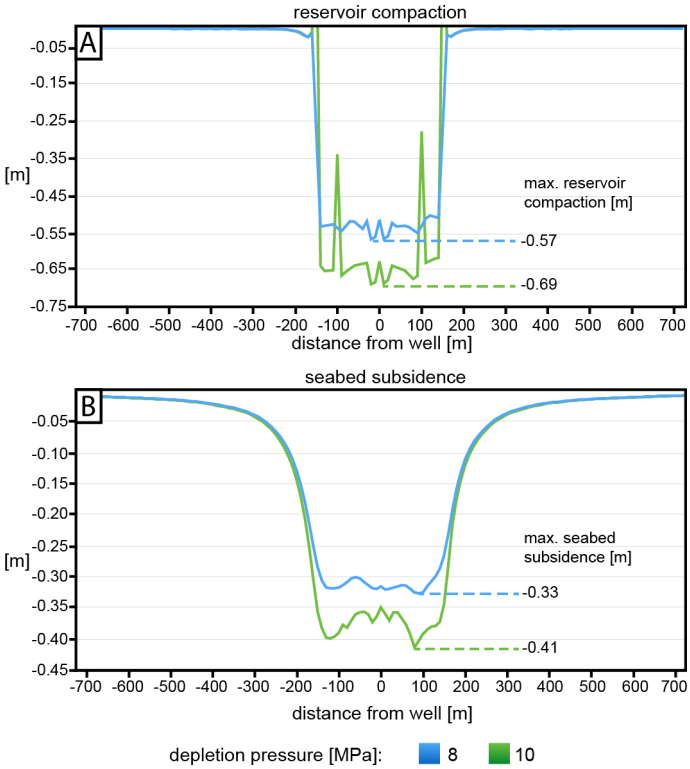

Fig. 5: Results from the parametric study for the shallow hydrate reservoir, showing reservoir compaction (A) and seabed subsidence (B) for depletion pressures of 8 and 10 MPa, assuming a maximum dissociation radius of 150 m around the borehole.

4.3.2 Production time

We simulated the production time by varying the size of the area affected by hydrate dissociation. Small radii of about several tens of meters around the well will be reached after a small production time of a few days (e.g. Kim et al., 2014, Konno et al., 2017), while the maximum case of a 150-m radius represents a longer production time of up to a few years. The dissociation area radii tested in this study varied between 10 m and 150 m. Fig. 6 shows the simulations for a maximum depletion pressure of 10 MPa. With increasing dissociation radius, the seabed subsidence increases both vertically and laterally. The lateral extent of the deformation remains in the vicinity of the compacted reservoir, but the vertical displacement at the seabed increases with the laterally spreading dissociation front in the reservoir (Fig. 6A). The FoS of the slip surface remains unaffected for the tested dissociation radii.

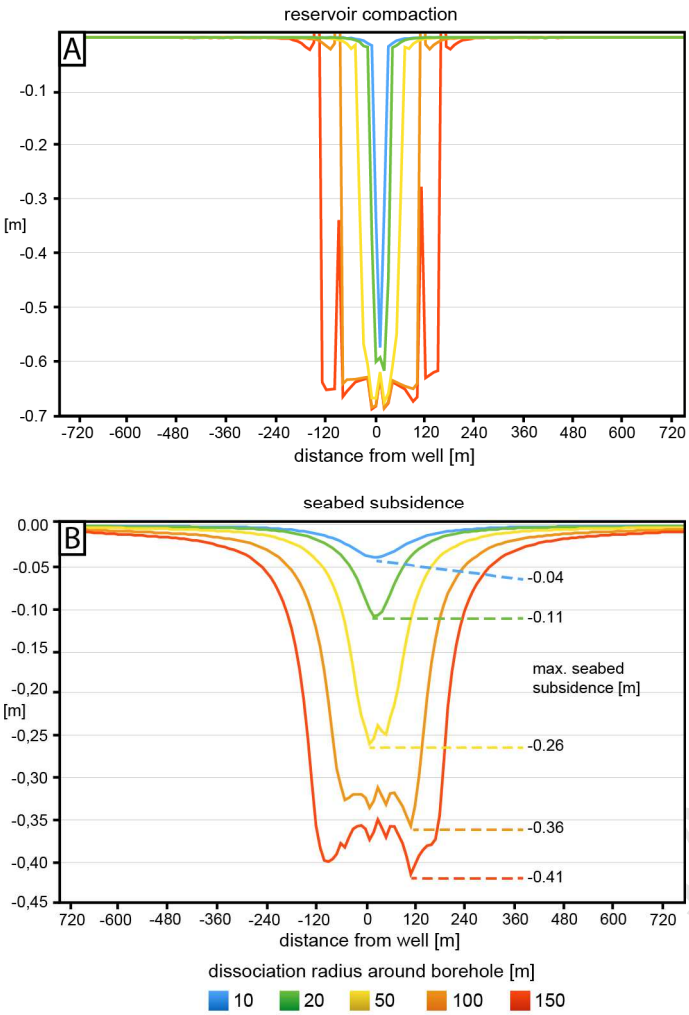

Fig. 6: Results from the parametric study for the shallow hydrate reservoir, showing reservoir compaction (A) and seabed subsidence (B) for a depletion pressure of 10 MPa for different hydrate dissociation radii around the borehole. The simulations indicate that the lateral extent of the subsided seafloor is directly coupled to the compacted reservoir.

4.3.3 Change of well locations

Moving the well location from the center of the channel (base case) 300 m closer to the levee wall (biased case) results in a shift of maximum displacements of the reservoir compaction and seabed subsidence. Fig. 7 shows the simulations for a 150 m dissociation front around the well and a depletion pressure of 8 MPa. Although closer to the levee and its failure surface, the deformation at the seabed does not spread out towards the slip surface and the FoS remains unaffected for the biased well location.

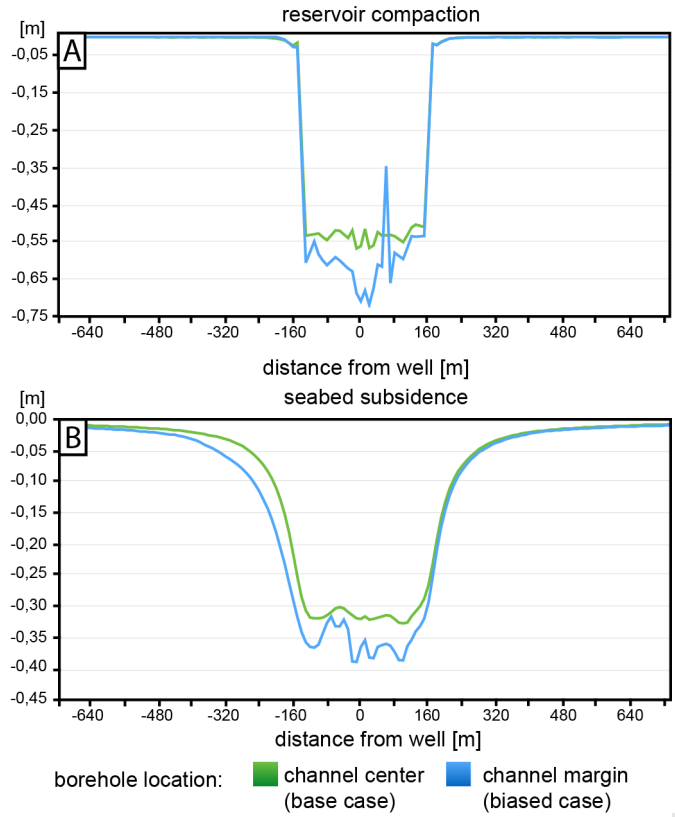

Fig. 7. Results from the parametric study, showing a comparison of reservoir compaction (A) and seabed subsidence (B) between two well locations in the channel center (base case) and the channel margin (biased case). The well locations are shown in Fig. 4C.

4.3.4 Reservoir depth

In order to compare production of a shallow reservoir in about 60 m depth with a deeper reservoir in about 140 m depth, we plotted the ratio of dissociation radius (representing production time) to depth of the reservoir against the ratio of maximum subsidence to maximum reservoir compaction (Fig. 8). Factors controlling the ratio of seabed subsidence to reservoir compaction are, e.g., depth and geometry of the reservoir, and the stiffness contrast between reservoir and overburden. If the dissociation radius is increasing (i.e. dissociation radius / reservoir depth is greater than 0.5), the production from the deep reservoir triggers slightly higher subsidence compared to the subsidence induced by production from the shallow reservoir (Fig. 8). In the early production stage, when the dissociation radius is smaller than 0.5 times the reservoir depth, the ratio of subsidence to compaction remains similar. The FoS of the slip surface remains unaffected at 1.27 for both reservoirs. Note that

the simulation for the deep reservoir was only tested for the maximum depletion pressure of 10 MPa.

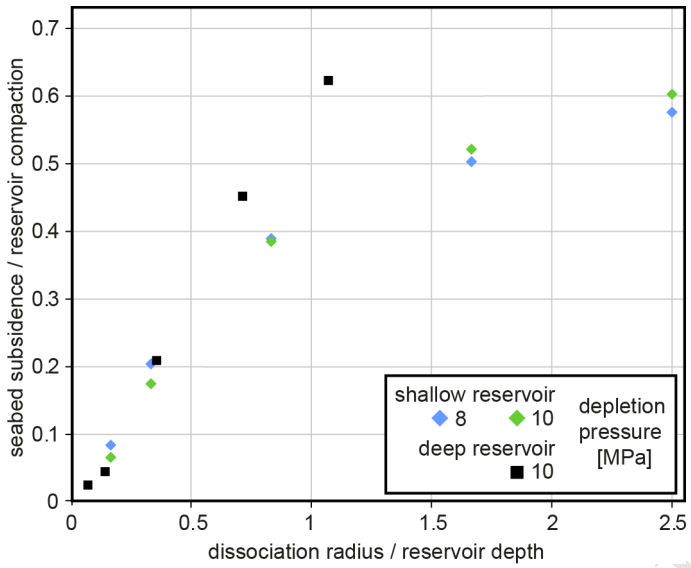

Fig 8: Results from the parametric study, showing a comparison of the two hypothetical reservoirs, with the shallow reservoir located at about 60 m depth and the deeper reservoir at about 140 m depth below the seafloor (Fig. 4A).

4.4 Landslide dynamics (quasi-2D)

The results of the landslide dynamic simulations using the 2D slope stability output showed that the run-out reaches approximately 500 – 900 m for the static case and 600 m – 1000 m in the pseudo-static case (Fig. 9). The final deposit reaches a thickness of approximately 5 m in the static case (Fig. 9C) and 6 m in the pseudo-static case (Fig. 9D). The flow velocity at the toe peaks at 9 m s^{-1} and 14 m s^{-1} with marginally higher velocities for the pseudo-static case compared to the static case (Figs. 9E, F). During the remobilization, the maximum thickness of the flow is in the order of 8 - 20 m for the static case and about 250 m away from the landslide toe at failure (Fig. 9G) with maximum flow velocities around 9 to 15 m s^{-1} (Fig. 9I). For the pseudo-static case, the maximum flow thickness is on average 3 m thicker due to the larger volume which is mobilized (Fig. 9H) with maximum flow velocities around 10 m s^{-1} to 16 m s^{-1} (Fig. 9J).

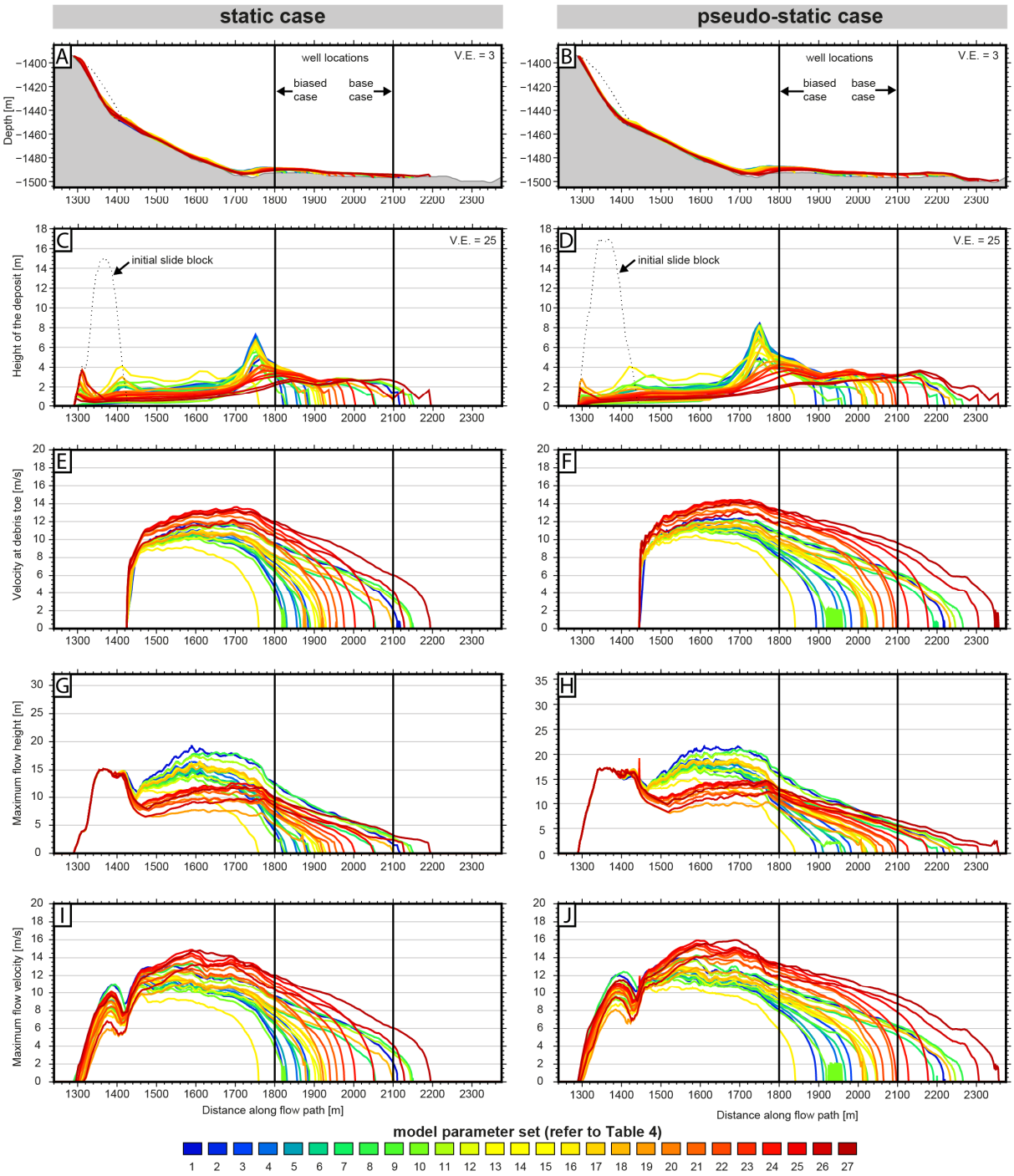

Fig 9: Results from the quasi-2D landslide dynamics simulation for the static (left) and pseudo-static (right) cases. The model parameters for the 27 different runs (color coded) are presented in table 4. A, B: Final deposit of the mass projected on the topography (grey). The initial slide block is shown as a dotted line. C, D: Final deposit (thickness of the mass along the flow path. E, F: toe velocities during the flow. G, H: peak height at each point along the flow path. I, J: peak velocity at each point along the flow path.

5. Discussion

5.1 Slope stability before, during and after productions

The parameters used for the screening and geomechanical analysis of the area are conservative (i.e. gearing the model towards less stable slopes), but in the absence of specific knowledge of the subsurface conditions, they provide effective screening criteria. The screening of the study area revealed that the entire area is essentially stable, with only some segments along the inner levee flanks of the paleo channels that appear critical. Here, slope angles exceed 9°, which results in a FoS of <1.5 against slope failure. For engineering works to be conducted, the FoS value is typically required to be above 1.5 in the static case and 1.1-1.2 in the pseudo-static case (e.g. Eurocode 8 (CEN, 2004), depending on the type of facility). In our study, the 2D slope stability analysis for the western levee of the SUGAR channel revealed a FoS of 1.27 in the static case, which is typically not sufficiently high. In the pseudo-static analysis, the FoS is 1.01, which is considered critical. In case of an earthquake, a landslide would likely occur. Compared to the static case, a larger volume of soil may be mobilized as the slip plane is located deeper and more wide-spread.

The preconditioning factors of slope instability considered in this study are the change in geometry due to seabed subsidence, and shear strength reduction due to the removal of solid hydrate from the hypothetic reservoir during production. However, the post-production landslide stability model, which takes these effects into account, shows that the deterministic FoS remains unchanged at 1.27. The production of gas out of the hypothetical methane hydrate reservoir therefore has no effect on slope stability. The main reason why the strength reduction does not affect the initial FoS is that the relatively shallow depth of the hydrate reservoir (60 m) is still deeper than the calculated line of failure. Seafloor subsidence, although amounting to 0.4 m, remains confined to the immediate vicinity above the production sites, which are located in relatively flat terrain several hundreds of meters away from the steep levee flanks. Production out of the deeper reservoir triggers a slightly higher

subsidence, which may be due to the different geometry and thickness (15 m) compared to the shallow reservoir (6 m). However, the ratio of subsidence to compaction remains similar when the dissociation radius is smaller than 0.5 times the reservoir depth (Fig. 8). Assuming a constant reservoir thickness and lateral extent, this observation indicates that the subsidence decreases with depth of the reservoir because of an arching effect. Thus, if the reservoir is located deep enough to achieve an arching effect, the hydrate dissociation becomes less critical for seabed subsidence and slope stability.

Because of the extent of the hydrate reservoir, there is no point in moving the well location closer to the levee flank. The slope has a length of about 300m, and therefore the estimated maximum subsidence would likely not impact the inclination of the levee even if hydrate production would occur directly below the slope. The small differences in model results for the two well locations (Fig. 7) are due to the differences in geometry and slightly inhomogeneous thickness of the reservoir at both locations.

5.2 Potential hazards related to slope instabilities in the target area

One of the major hazards in the study area is the triggering of a landslide (i.e. by an earthquake). The analysis of landslide dynamics carried out in this study showed that a hypothetical slide may impact potential seafloor installations in both the base and the biased scenarios. The final slide deposit extends to the center of the channel with a depositional height of up to 5-6 m. In the base case the deposit may therefore reach the well (static case), and extend even beyond the well in the pseudo-static simulation. In the biased case, in which the well is located closer to the levee flank, the debris flow would reach the well site at a velocity of 4-12 m s^{-1}. Thus, a production platform would have to be strong enough to withstand such an impact or drilling has to be conducted at sufficiently great distance to the levee flank. Because the entire inner levee flank in this area dips at rather uniform steep angles, this recommendation does not only apply to the location of the 2D slope stability model, but also in upward or downward direction along the channel. In shallower water, the

levee slopes generally become steeper which negatively affects the FoS. Further, many landslides in river deltas have a multiphase and retrogressive development (Kvalstad et al., 2005, Kvalstad, 2007). After failure, the new slope may also be unstable and fail progressively in a back-stepping process over a relatively short period.

5.3 Limitations

In the absence of in-situ geotechnical properties, several approximations and simplifications had to be made in order to create a geomechanical model for the study area. The largest uncertainty stems from the actual distribution of the gas hydrates as well as the in-situ hydrate saturation. Changes of these parameters will have an impact on the modeling results and the assessment of geohazards. It is therefore necessary to obtain more accurate estimates of hydrate saturation through geophysical inversion of the existing data and future well logs to better constrain the amount and distribution of gas hydrates in the Danube deep-sea fan. Furthermore, the actual pore pressure distribution in the sediments is unknown and was therefore not considered in this study. Zones of overpressure may change the seafloor stability significantly since the effective stress (and therefore the shear strength) decreases with increasing pore pressure (e.g. Riboulot et al., 2016).

The model presented in this study consists of an isolated reservoir with constant pressure within the dissociation radius around the borehole. However, simulations showed that the target depletion pressure is only reached in a very narrow area around the well and decreases with further distance from the well (Kim et al., 2014, Konno et al., 2017). In this sense, the results presented in this study provide conservative estimates of slope stability changes. Transient behavior of hydrate dissociation was not considered in this study. Consequently, the simulation (assuming steady-state conditions) assesses only the most critical hazard of subsidence in a conservative way.

The applied mean depletion pressure of e.g. 10 MPa for the entire reservoir is considered representative for a higher depletion pressure target at the borehole (e.g. 12 MPa).

A production simulation carried out for the Nankai hydrate production site found that a stepwise production method with waiting times in the order of ten days between two pressure reductions helps to reduce ground settlements (Zhou et al., 2014). Such a delayed depressurization process reduces gas production in the short term, but in the long-term, the total amount of produced gas will be similar to scenarios where the pressure target is achieved immediately.

The slope stability model was simplified by using a 2D geometry, because the most critical slope angles along the levee walls parallel to the 2D profile are rather similar (Fig. 3). However, the FoS can be rather sensitive to small differences in slope geometry if the preliminary FoS is considered critical. In this study, the potential for shallow seated small failures may be neglected due to the 10-m grid size of the bathymetric data. We also neglected the effect of the sloping seabed in the direction of the channel. Only a more sophisticated approach based on a 3D geometry model would give certainty as to the predicted failure loads in this complex bathymetric setting. A comparison between a 2D and a 3D approach for a different study area is e.g. presented in Sultan et al. (2011).

Finally, our modelling did not take into account fluid coupling of chemical disequilibrium. However, considering the uncertainties mentioned above, such in-depth modelling is currently not feasible but should be considered in a future model when more data becomes available.

6. Conclusions

The combined geomechanical analyses carried out in this study include slope stability investigations, analysis of landslide dynamics, and consequences of gas hydrate production on reservoir compaction and seabed subsidence, which may lead to secondary failures along the slope. The models were constrained from geophysical data combined with sparse geotechnical data. Screening indicated that the area may be considered stable in general, with critical

slopes encountered at the inner levee flanks which are present along numerous paleo channel courses throughout the Danube deep-sea fan. The 2D slope stability modeling in the vicinity of a hypothetical gas hydrate reservoir in about 60 m below the seafloor suggests that the area is relatively safe against slope failure under static conditions (FoS around 1.27), but probably not sufficiently safe to allow developments of infrastructure at the seabed without taking specific mitigation measures into account. The simulation of hydrate production showed that the FoS is not significantly affected by the production process, as reservoir compaction and seabed subsidence remain confined to the immediate vicinity of the well sites, which lie in a sufficient distance from the main critical instability zone at the levee flank. The landslide dynamic simulation showed that if slope failure were to happen, the mobilized mass could impact at the production sites. It is more likely that seafloor facilities are damaged by a landslide triggered by an earthquake during drilling than by a landslide triggered by production itself. In general, it may be sufficient to keep a large enough distance away from the steep levee flanks to avoid any hydrate production-related slope failures.

Uncited references

Kwon et al. (2010)

Kwon et al. (2011)

Cha et al. (2016)

Acknowledgements

The research leading to these results has received funding from the European Union Seventh Framework Programme (FP7/2007-2013) under the MIDAS project, grant agreement no. 603418, from the German Ministry of Education and Research (BMBF) and from the Federal Ministry of Economy and Energy (BMWi) through the SUGAR project (grant nos. 03G0819A, 03SX320A, 03G0856A). We would like to thank the captains and crews of RV MARIA S. MERIAN and RV Pourquoi Pas? cruises MSM34 and GHASS as well as the lab technicians for their excellent support. We further acknowledge Sebastien Garziglia for the

analysis on the overburden soil parameters and Dieter Issler and Noel Boylan for developing the landslide dynamics code partly supported by NGI's internal R&D funding. Two anonymous reviewers and the editor Valentina Blinova are thanked for constructive feedback and comments that greatly improved this paper.

References

Bialas, J., Klaucke, I., and Haeckel, M. (Eds.), 2014. FS MARIA S. MERIAN Fahrtbericht / Cruise Report MSM-34/1 & 2 - SUGAR Site, 06.12.13-16.01.14, Varna – Varna. GEOMAR Report, N. Ser. 015. GEOMAR Helmholtz-Zentrum für Ozeanforschung Kiel, Germany, 111 pp., doi:10.3289/GEOMAR_REP_ NS_15_2014.

Boswell, R., 2009. Is gas hydrate energy within reach? Science 325, pp. 957-958, doi:10.1126/science.1175074.

Brinkgreve, R.B.J., Broere, W., and Waterman, D., 2007. PLAXIS 2D Manual. Delft University of Technology, Delft.

Carlton, B.D., Price, K., Vanneste, M., and Forsberg, C.F., 2017. Development and application of a regional slope stability assessment screening tool. 2nd International Workshop on Landslides in Sensitive Clays, Trondheim, Norway, 10 pp.

CEN, 2004. EN-1998-1: Eurocode 8: Design of Structures for Earthquake Resistance. European Committee for Standardization, Brussels, 229 pp.

Cha, Y., Yun, T.S., Kim, Y.J., Lee, J.Y., and Kwon, T.H., 2016. Geomechanical, hydraulic and thermal characteristics of deep oceanic sandy sediments recovered during the second Ullueng Basin Gas Hydrate Expedition. Energies 9, 23 pp., doi:10.3390/en9100775.

Crutchley, G.J., Mountjoy, J.J., Pecher, I.A., Gorman, A.R., and Henrys, S.A., 2016. Submarine slope instabilities coincident with shallow gas hydrate systems: Insights from New Zealand examples. In: Lamarche, G., Mountjoy, J., Bull, S., Hubble, T., Krastel, S., Lane, E., Micallef, A., Moscardelli, L., Mueller, C., Pecher, I., and Woelz,

S. (Eds.), Submarine Mass Movements and their Consequences. Advances in Natural and Technological Hazards Research 41, Springer, pp. 401-409.

Damuth, J.E., 2002. The Amazon-HARP Fan model: Facies distributions in mud-rich deep-sea fans based on systematic coring of architectural elements of Amazon Fan. CIESM Workshop 17, pp 19-22.

Dannowski, A., Bialas, J., Zander, T., and Klaeschen, D., 2016. Shear wave modelling of high-resolution OBS data in a gas hydrate environment in the Danube deep-sea fan, Black Sea. AGU Fall Meeting 2016, San Francisco, USA, 12-16 December 2016.

De Blasio, F.V., Engvik, L., Harbitz, C., and Elverhøi, A., 2004. Hydroplaning and submarine debris flows. Journal of Geophysical Research: Oceans 109, C01002, doi:10.1029/2002JC001714.

Degens, E.T., and Ross, D.A., 1974. The Black Sea – Geology, Chemistry, and Biology. The American Association of Petroleum Geologists, Tulsa, USA.

Fjaer, E., Holt, R.M., Horsrud, P., Raaen, A.M., and Risnes, R., 2008. Petroleum Related Rock Mechanics (Second Edition). Developments in Petroleum Science 53, Elsevier.

Garziglia, S., 2016. MIDAS. Complete geo-mechanical properties of gas hydrate bearing sediments from in situ geotechnical measurements. Scientific report, Ifremer, France, 22 pp.

Giardini, D., 1999. The global seismic hazard assessment program (GSHAP) – 1992/1999. Annali di Geofisica 42, pp. 957-974.

Griffiths, D.V., and Lane, P.A., 1999. Slope stability analysis by finite elements. Geotechnique 49, pp. 387-403.

Hansen, L.A.S., Callow, R.H.T., Kane, I.A., Gamberi, F., Rovere, M., Cronin, B.T., and Kneller, B.C., 2015. Genesis and character of thin-bedded turbidites associated with submarine channels. Marine and Petroleum Geology 67, pp. 852-879, doi:10.1016/j.marpetgeo.2015.06.007.

Hynes-Griffin, M.E., and Franklin, A.G., 1984. Rationalizing the seismic coefficient method. US Army Corps of Engineers Waterways Experiment Station. Miscellaneous Paper vol. GL-84-13, 41 pp.

Imram, J., Harff, P., and Parker, G., 2001. A numerical model of submarine debris flow with graphical user interface. Computers & Geosciences 27, pp. 717-729, doi:10.1016/S0098-3004(00)00124-2.

Ker, S., and Riboulot, V., 2015. GHASS cruise report. Ifremer, France, 53 pp.

Kim, A.R., Cho, G.C., Song, K.I., and Kim, S.J., 2014. Settlement prediction in the Ulleung Basin due to gas hydrate production. Offshore Technology Conference, OTC25308-MS, Houston, Texas, USA, 5-8 May 2014, 10 pp.

Konno, Y., Fujii, T., Sato, A., Akamine, K., Naiki, M., Masuda, Y., Yamamoto, K., and Nagao, J., 2017. Key findings of the world's first offshore methane hydrate production test off the coast of Japan: Toward future commercial production. Energy & Fuels 31, pp. 2607-2616, doi:10.1021/acs.energyfuels.6b03143.

Kvalstad, T.J., Andresen, L., Forsberg, C.F., Berg, K., Bryn, P., and Wangen, M., 2005. The Storegga slide: evaluation of triggering sources and slide mechanics. Marine and Petroleum Geology 22, pp. 245-256, doi:10.1016/j.marpetgeo.2004.10.019.

Kvalstad, T.J., 2007. What is the current "best practice" in offshore geohazard investigations? A state-of-the-art review. Offshore Technology Conference, OTC18545, Houston, Texas, USA, 30 April - 3 May 2007, 14 pp.

Kvalstad, T.J., Yamamoto, K., Noguchi, S., Uchida, S., and Soda, K., 2011. Effect of gas hydrate production on seabed stability in the eastern Nankai Trough area. Proceedings of the 7th International Conference on Gas Hydrates (ICGH), Edinburgh, Scotland, 17-21 July 2011, 10 pp.

Kwon, T.H., Song, K.I., and Cho, G.C., 2010. Destabilization of marine gas hydrate-bearing sediments induced by a hot wellbore: A numerical approach. Energy and Fuels 24, pp. 5493-5507, doi:10.1021/ef100596x.

Kwon, T.H., Lee, K., Cho, G.C., and Lee, J.Y., 2011. Geotechnical properties of deep oceanic sediments recovered from the hydrate occurrence regions in the Ulleung Basin, East Sea, Offshore Korea. Marine and Petroleum Geology 28, pp. 1870-1883, doi:10.1016/j.marpetgeo.2011.02.00315.

Kwon, T.H., and Cho, G.C., 2012. Submarine slope failure primed and triggered by bottom water warming in oceanic hydrate-bearing deposits. Energies 5, pp. 2849-2873, doi: 10.3390/en5082849.

Matova, M., 2000. Recent geological activity along the northeastern Bulgarian Black Sea coast. Geological Quaterly 44, pp. 355-362.

Merey, S., and Sinayuc, C., 2016a. Experimental set-up design for gas production from the Black Sea gas hydrate reservoirs. Journal of Natural Gas Science and Engineering 33, pp. 162-185, doi:10.1016/ j.jngse.2016.04.030.

Merey, S., and Sinayuc, C., 2016b. Investigation of gas hydrate potential of the Black Sea and modelling of gas production from a hypothetical Class 1 methane hydrate reservoir in the Black Sea conditions. Journal of Natural Gas Science and Engineering 29, pp. 66-79, doi: 10.1016/j.jngse.2015.12.048.

Micallef, A., Masson, D.G., Berndt, C., and Stow, D.A.V., 2009. Development and mass movement processes of the north-eastern Storegga Slide. Quaternary Science Reviews 28, pp. 433-448, doi:10.1016/ j.quascirev.2008.09.026.

Morgenstern, N.R., 1967. Submarine slumping and the initiation of turbidity currents. In: Richards, A.F. (Ed.), Marine Geotechnique. University of Illinois Press, Urbana, Illinois, pp. 189-210.

Myshakin, E.M., Gaddipati, M., Rose, K., and Anderson, B.J., 2012. Numerical simulations of depressurization-induced gas production from gas hydrate reservoirs at the Walker Ridge 313 site, northern Gulf of Mexico. Marine and Petroleum Geology 34, pp. 169-185, doi:10.1016/j.marpetgeo.2011.09.001.

Özsoy, E., and Ünlüata, Ü., 1997. Oceanography of the Black Sea: a review of some recent results. Earth-Science Reviews 42, pp. 231-272, doi:10.1016/S0012-8252(97)81859-4.

Popescu, I., Lericolais, G., Panin, N., Wong, H.K., and Droz, L., 2001. Late Quaternary channel avulsions on the Danube deep-sea fan, Black Sea. Marine Geology 179, pp. 25-37, doi:10.1016/S0025-3227(01)00197-9.

Popescu, I., De Batist, M., Lericolais, G., Nouzé, H., Poort, J., Panin, N., Versteeg, W., and Gillet, H., 2006. Multiple bottom-simulating reflections in the Black Sea: Potential proxies of past climate conditions. Marine Geology 227, pp. 163-176, doi:10.1016/j.margeo.2005.12.006.

Riboulot, V., Cattaneo, A., Sultan, N., Garziglia, S., Ker, S., Imbert, P., and Voisset, M., 2013. Sea-level change and free gas occurrence influencing a submarine landslide and pockmark formation and distribution in deepwater Nigeria. Earth and Planetary Science Letters 375, pp. 78-91, doi:10.1016/j.epsl.2013.05.013.

Ross, D.A., and Degens, E.T., 1974. Recent sediments of Black Sea. In: Degens, E.T., Ross, D.A. (eds.), The Black Sea – Geology, Chemistry, and Biology. American Association of Petroleum Geologists, pp. 183-199.

Saeki, T., Fujii, T., Inamori, T., Kobayashi, T., Hayashi, Nagakubo, S., and Takano, O., 2008. Extraction of methane hydrate concentrated zone for resource assessment in the Eastern Nankai Trough, Japan. Offshore Technology Conference, OTC19311, Houston, Texas, USA, 5-9 May 2008, 8 pp.

Santamarina, J.C., Dai, S., Terzariol, M., Jang, J., Waite, W.F., Winters, W.J., Nagao, J., Yoneda, J., Konno, Y., Fujii, T., and Suzuki, K., 2015. Hydro-bio-geomechanical

properties of hydrate-bearing sediments from Nankai Trough. Marine and Petroleum Geology 66, pp. 434-450, doi:10.1016/j.marpetgeo.2015.02.033.

Schwalenberg, K., Gehrmann, R., Rippel, D., Hölz, S., and Zander, T., 2016. Gas hydrate saturation estimates from the Danube Delta offshore Romania using marine controlled source electromagnetics. GIMS13 Gas in Marine Sediments, Tromsø, Norway, 19-22 September 2016.

Shipley, T. H., Houston, M. H., and Buffler, R. T., 1979. Seismic evidence for widespread occurrence of possible gas-hydrate horizons on continental slopes and rises. AAPG Bulletin 63, pp. 2204-2213.

Sloan, E.D., 1998. Clathrate Hydrates of Natural Gases. Marcel Dekker, New York.

Soulet, G., Delaygue, G., and Vallet-Coulomb, C., 2010. Glacial hydrologic conditions in the Black Sea reconstructed using geochemical pore water profiles. Earth and Planetary Science Letters 296, pp. 57-66, doi:10.1016/j.epsl.2010.04.045.

Sultan, N., Garziglia, S., and Colliat, J.L., 2011. Gas hydrate occurrences and seafloor deformation: Investigation of strain-softening of gas-hydrate bearing sediments and its consequence in terms of submarine slope instabilities. Offshore Technology Conference, OTC21294, Houston, Texas, USA, 2-5 May 2011, 18 pp.

Urlaub, M., Talling, P.J., and Masson, D.G., 2013. Timing and frequency of large submarine landslides: implications for understanding triggers and future geohazard. Quaternary Science Reviews 72, pp. 63-82, doi:10.1016/j.quascirev.2013.04.020.

Vanneste, M., Harbitz, C.B., De Blasio, F.V., Glimsdal, S., Mienert, J., and Elverhøi, A, 2011. Hinlopen-Yermak Landslide, Arctic Ocean – Geomorphology, Landslide Dynamics, and Tsunami Simulations. In: Shipp, R.C., Weimer, P., and Posamentier, H. (Eds.), Mass-Transport Deposits in Deepwater Settings. Society for Sedimentary Geology, Tulsa, Oklahoma, USA, pp. 509-527.

Vanneste, M., Sultan, N., Garziglia, S., Forsberg, C.F., and L'Heureux, J.S., 2014. Seafloor instabilities and sediment deformation processes: The need for integrated, multi-disciplinary investigations. Marine Geology 352, pp. 183-214, doi:10.1016/j.margeo.2014.01.005.

Waite, W.F., Santamarina, J.C., Cortes, D.D., Dugan, B., Espinoza, D.N., Germaine, J., Jang, J., Jung, J.W., Kneafsey, T.J., Shin, H., Soga, K., Winters, W.J., and Yun, T.S., 2009. Physical properties of hydrate-bearing sediments. Reviews of Geophysics 47, RG4003, doi:10.1029/2008RG000279.

Wong, H.K., Winguth, C., Panin, N., Dinu, C., Wollschläger, M., Georgescu, P., Ungereanu, G., Krugliakov, V.V., and Podshuveit, V., 1997. The Danube and Dniepr fans, morphostructure and evolution. GeoEcoMarina 2, pp. 77-102.

Yamamoto, K., Terao, Y., Fujii, T., Ikawa, T., Seki, M., Matsuzawa, M., and Kanno, T., 2014. Operational overview of the first offshore production test of methane hydrates in the Eastern Nankai Trough. Offshore Technology Conferency, OTC25243-MS, Houston, Texas, USA, 5-8 May 2014, 11 pp.

Yoneda, J., Masui, A., Konno, Y., Jin, Y., Egawa, K., Kida, M., Ito, T., Nagao, J., and Tenma, N., 2015. Mechanical properties of hydrate-bearing turbidite reservoir in the first gas production test site of the Eastern Nankai Trough. Marine and Petroleum Geology 66, pp. 471-486, doi:10.1016/ j.marpetgeo.2015.02.029.

Zander, T., Haeckel, M., Berndt, C., Chi, W.C., Klaucke, I., Bialas, J., Klaeschen, D., Koch, S., and Atgın, O., 2017. On the origin of multiple BSRs in the Danube deep-sea fan, Black Sea. Earth and Planetary Science Letters 462, pp. 15-25, doi:10.1016/j.epsl.2017.01.006.

Zhou, M., Soga, K., Xu, E., Uchida, S., and Yamamoto, K., 2014. Numerical study on Eastern Nankai Trough gas hydrate production test. Offshore Technology Conference, OTC25169, Houston, Texas, USA, 5-8 May 2014, 19 pp.

Highlights

1. The Danube deep-sea fan offers best conditions for hydrate production
2. Gas production out of a hypothetical methane hydrate reservoir was simulated
3. Hazard assessment to investigate the hazard of production-induced slope failures
4. Factor of Safety against slope failure is not affected by the production process
5. Mobilized mass could hit the production site if landslide were to happen